Heliyon 6 (2020) e05813

Contents lists available at ScienceDirect

Heliyon

journal homepage: www.cell.com/heliyon

Research article

# Synthesis of $Fe_3O_4$/Ag nanohybrid ferrofluids and their applications as antimicrobial and antifibrotic agents

Ahmad Taufiq [a,*], Rosy Eko Saputro [a], Hendra Susanto [b], Nurul Hidayat [a], Sunaryono Sunaryono [a], Tahta Amrillah [c], Husni Wahyu Wijaya [d], Nandang Mufti [a], Firman Mangasa Simanjuntak [e]

[a] Department of Physics, Faculty of Mathematics and Natural Sciences, Universitas Negeri Malang, Jl. Semarang 5, Malang, 65145, Indonesia
[b] Department of Biology, Faculty of Mathematics and Natural Sciences, Universitas Negeri Malang, Jl. Semarang 5, Malang, 65145, Indonesia
[c] Department of Physics, Faculty of Science and Technology, Universitas Airlangga, Surabaya, 60115, Indonesia
[d] Department of Chemistry, Faculty of Mathematics and Natural Sciences, Universitas Negeri Malang, Jl. Semarang 5, Malang, 65145, Indonesia
[e] Zepler Institute for Photonics and Nanoelectronics, University of Southampton, Southampton, SO17 1BJ, United Kingdom

ARTICLE INFO

*Keywords:*
$Fe_3O_4$/Ag
Double-layered ferrofluid
Antimicrobial
Antifibrosis

ABSTRACT

To date, the search for creating stable ferrofluids with excellent properties for biomedical application is one of the challenging scientific and practical investigations. In this study, novel $Fe_3O_4$/Ag nanohybrid ferrofluids from iron sand were synthesized using a double-layer method. The $Fe_3O_4$/Ag nanocomposites exhibited stable crystallite sizes of 11.8 12.1 nm and 36.8–37.2 nm for $Fe_3O_4$ and Ag, respectively. The lattice parameters of the spinel structure $Fe_3O_4$ and face-centered cubic Ag were respectively 8.344 Å and 4.091 Å. With increasing Ag amount, the crystallite phase of Ag in the nanocomposites increased from 40.2% to 77.2%. The XPS results confirmed that $Fe_3O_4$/Ag nanocomposites were successfully prepared, where $Fe_3O_4$ mixed well with Ag via strong ionic bonding. The FTIR results confirmed the presence of $Fe_3O_4$/Ag, oleic acid, and dimethyl sulfoxide as the filler, first layer, and second layer, respectively. The as-prepared ferrofluids exhibited superparamagnetic behavior, where the saturation magnetization decreased with increasing Ag content. The $Fe_3O_4$/Ag nanohybrid ferrofluids exhibited excellent antimicrobial performance against *Bacillus subtilis*, *Staphylococcus aureus*, *Escherichia coli*, and *Candida albicans*. More importantly, the $Fe_3O_4$/Ag nanohybrid ferrofluids decreased the progression of liver fibrosis-related inflammation and fibrogenic activity on hepatic stellate cells.

## 1. Introduction

Over the past few years, multifunctional nanohybrid ferrofluids have aroused remarkable interest because of their unique characteristics, including excellent magnetic properties of stable liquid phases. Theoretically, ferrofluids are stable colloidal suspensions that contain single-domain magnetic nanoparticles as fillers dispersed in an appropriate carrier liquid [1]. Ferrofluids are considered smart materials because of their outstanding combination of features such as flexible flowability, rapid magnetic response, and tunable optical and thermal characteristics [2]. Therefore, many researchers in the nanoscience and nanotechnology fields have developed ferrofluids for use in, for example, hyperthermia cancer treatments, magnetic resonance imaging contrast agents [3], antimicrobial agents [4, 5], and liver fibrosis treatments [6].

In biomedical applications, ferrofluids with $Fe_3O_4$ nanoparticles as the magnetic fillers have been fabricated because $Fe_3O_4$ nanoparticles exhibit properties superior to those of other materials, such as superparamagnetism, a high surface-to-volume ratio, easy magnetic separation [7], and good biocompatibility. Such fabrication can be found in previous studies related to the structural modification and synthesis method of $Fe_3O_4$ nanoparticles [8, 9, 10]. However, $Fe_3O_4$ nanoparticles are likely to agglomerate, resulting in the loss of active surface area and diminished biomedical performance [11], including antimicrobial and liver fibrosis treatments. In addition, $Fe_3O_4$ nanoparticles have a low ability to penetrate bacterial or fungal membranes, which restricts their ability to inhibit microbial growth [12]. $Fe_3O_4$ nanoparticles also tend to be easily oxidized, which adversely affects their physical and chemical stability [13]. Therefore, in the present study, we combine $Fe_3O_4$ nanoparticles with Ag, which exhibits excellent antimicrobial performance, by preparing $Fe_3O_4$/Ag nanocomposites as the fillers in ferrofluids. Ag was chosen because it can prevent the agglomeration of $Fe_3O_4$ nanoparticles [14]. Furthermore, the combination of Ag and Fe ions in $Fe_3O_4$/Ag

* Corresponding author.
*E-mail address:* ahmad.taufiq.fmipa@um.ac.id (A. Taufiq).

https://doi.org/10.1016/j.heliyon.2020.e05813
Received 1 August 2020; Received in revised form 25 October 2020; Accepted 18 December 2020

hybrid nanocomposites should, in principle, lead to substantial antimicrobial activity. The selection of Ag is also based on its superior disinfectant properties compared with those of other metals [15]. Hence, the combination of $Fe_3O_4$ and Ag in the ferrofluids is expected to result in enhanced ability to inhibit the growth of various bacterial, fungal, and viral pathogens [16].

Another important issue when preparing ferrofluids is how to solve the difficulty of maintaining their stability. Ferrofluid stability plays a critical role in biomedical applications, particularly in their antimicrobial efficacy and liver fibrosis treatment. A recent study has shown that increasing the stability of ferrofluids significantly enhances their antimicrobial performance against *Bacillus subtilis*, *Staphylococcus aureus*, *Escherichia coli*, and *Candida albicans* [17]. The classic problem that causes difficulty in attaining stable ferrofluids is the tendency of $Fe_3O_4$ to agglomerate as a result of van der Waals forces [18], which interfere with the single-domain formation of magnetic nanoparticles. Thus far, to solve such problems, extensive effort has been devoted to coating the fillers in ferrofluids with various surfactants, such as oleic acid [13], other carboxylic acids [19], and tetramethylammonium ion [20], using a monolayer technique. In principle, surfactants were subject to coat magnetic nanoparticle fillers so that they remain stable under an external magnetic field [21]. However, the incorporation of only one surfactant did not sustain the ferrofluids stability in the long run [22]. The instability of ferrofluids leads to undesirable effects when they are used in biomedical applications, including malfunction and reduced antimicrobial performance against microbial pathogens [23]. Consequently, long-term stability of ferrofluids is one of important requirements for their application in the biomedical field.

The use of ferrofluids in advanced biomedical applications is considered as a new approach in the detection of liver cancer development based on the progression of liver fibrosis and cirrhosis. The magnetic nanoparticles, as the main component in ferrofluids, are able to detect the liver injury-associated hepatic stellate cells (HSC) activity at different stages of liver fibrosis [24]. The iron oxide nanoparticles treatment can inhibit liver fibrosis in HSC [25] and induce ferroptosis [26]. Although the magnetic nanoparticles are potentially great for clinical therapies [27], however, there is no adequate report on how ferrofluids can control the physiological performance of liver-related fibrosis. Therefore, this present study aims to substantially enhance the antimicrobial performance and liver fibrosis treatment using stable ferrofluids with $Fe_3O_4$/Ag nanocomposite fillers. We prepared $Fe_3O_4$/Ag nanohybrid ferrofluids using respectively oleic acid and dimethyl sulfoxide (DMSO) as the first and second surfactant layers. The first layer was chosen because it is nontoxic, biocompatible, and able to stabilize fillers to minimize agglomeration [28]. The second surfactant was used to support the first layer and further enhance the performance of $Fe_3O_4$/Ag nanocomposite fillers in biomedical applications [29]. In addition, we developed a simple synthesis method to fabricate $Fe_3O_4$/Ag nanohybrid ferrofluids using an abundant and inexpensive natural resource iron sand as the main precursor.

## 2. Experimental methods

### 2.1. Materials

Iron sand was used as the main source to produce $Fe_3O_4$ nanoparticles. Other materials included hydrochloric acid (HCl, 12 M), ammonium hydroxide ($NH_4OH$, 6.5 M), silver nitrate ($AgNO_3$), polyvinyl pyrrolidone (PVP), sodium borohydride ($NaBH_4$), sodium hydroxide (NaOH), oleic acid, and DMSO (14.1 M). All commercial materials were obtained from Merck in analytical grade and were used without further purification. Olive oil, which was used as a carrier liquid, was purchased from Borges.

### 2.2. Synthesis of $Fe_3O_4$/Ag nanohybrid ferrofluids

The first step in the synthesis of $Fe_3O_4$/Ag nanohybrid ferrofluids was the preparation of $Fe_3O_4$ from natural iron sand. The iron sand was first washed using distilled water and then dried under sunlight. The dried sand was filtered and separated using a magnetic bar to obtain $Fe_3O_4$ powder. Twenty grams of natural $Fe_3O_4$ was reacted with 58 mL of HCl for 30 min using a magnetic stirrer with a stirring rate at 600 rpm to

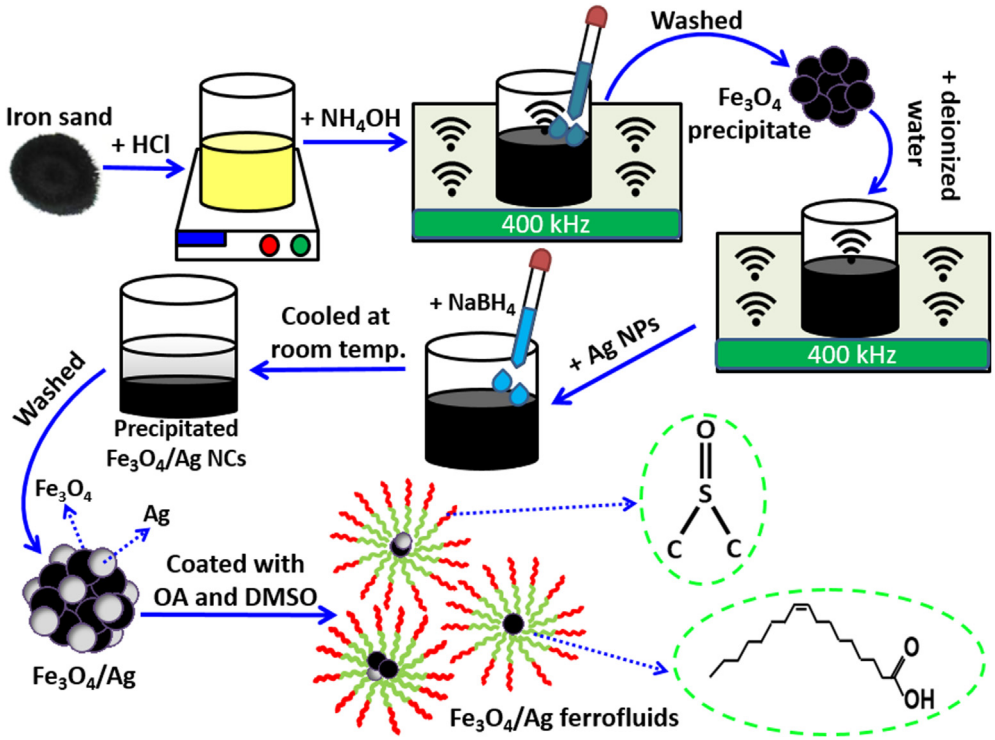


**Figure 1.** Synthesis scheme of the $Fe_3O_4$/Ag nanohybrid ferrofluids.

produce a $FeCl_2$–$FeCl_3$ solution. Twenty-five milliliters of $NH_4OH$ was titrated into the solution as it was sonicated in an ultrasonic bath at a frequency of 420 kHz for 20 min, which resulted in a black precipitate. The precipitate was washed to obtain $Fe_3O_4$ sediment. Meanwhile, Ag nanoparticles were prepared by dissolving 0.95 g of PVP into 465 mL of distilled water using a magnetic stirrer with a stirring rate at 400 rpm. The solution, labeled as "A", was inserted into an ice bath and maintained in the temperature range 5–10 °C. At the same time, 1.2 g of $AgNO_3$ was added to 10 mL of distilled water and then mixed with solution A in the ice bath using a magnetic stirrer, resulting in a homogenous solution labeled as "B". $NaBH_4$ as a reducing agent and NaOH as a stabilizer were titrated into solution B until a blackish-brown mixture was obtained. This mixture was covered with plastic wrap and stored for 24 h to form a black–grey precipitate. The precipitate was separated from the liquid using filter paper and then heated at 100 °C in an air atmosphere to obtain Ag nanoparticles. One gram of $Fe_3O_4$ precipitate obtained from the previous step was added to 50 mL of deionized water and sonicated for 10 min at a frequency of 400 kHz. Ag nanoparticles (1, 1.1, 1.2, 1.3, or 1.4 g) were then added, and the resultant mixture was stirred for 60 min. This mixture was then titrated with $NaBH_4$ while being stirred with a magnetic stirrer at 90 °C until a pH of 11 was achieved. The reaction temperature was then lowered to room temperature until the nanocomposite precipitate formed. The precipitate was subsequently washed until it reached a neutral pH. The precipitates obtained with Ag nanoparticle contents of 1, 1.1, 1.2, 1.3, and 1.4 g were respectively labeled as FA1, FA2, FA3, FA4, and FA5.

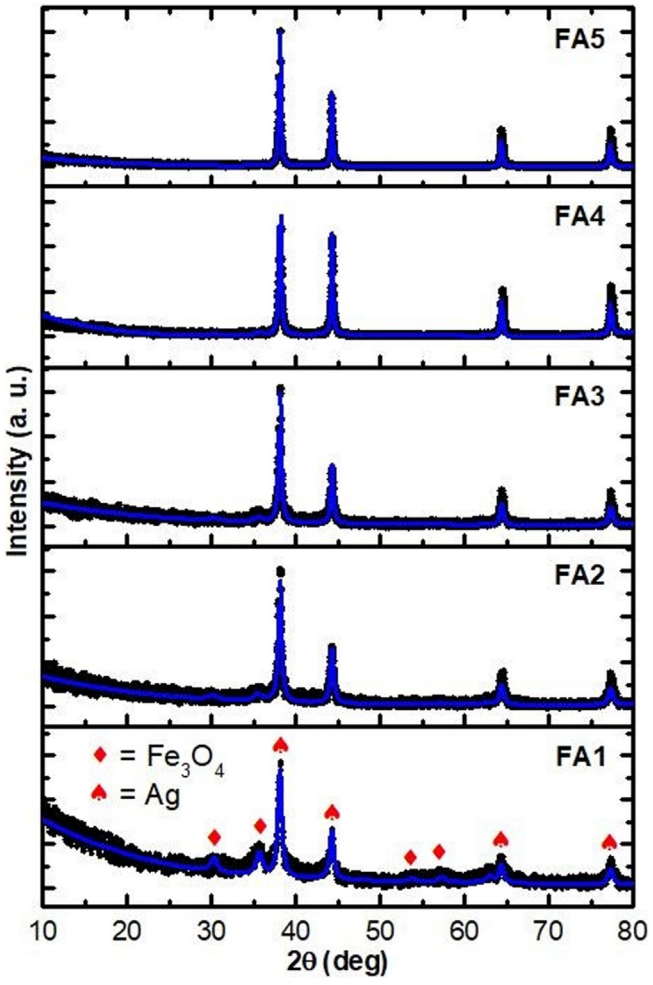


**Figure 2.** XRD patterns of the $Fe_3O_4$/Ag nanocomposites. The amount of Ag used in the synthesis increased from FA1 to FA5.

$Fe_3O_4$/Ag ferrofluids were prepared by reacting 1 g of FA1-FA5 samples with 2 mL of oleic acid using a magnetic stirrer at a temperature of 90 °C for 1 h. The mixture was then cooled to room temperature and mixed with DMSO, which formed a double surfactant layer. The obtained products were dispersed in olive oil as a carrier liquid to form $Fe_3O_4$/Ag nanohybrid ferrofluids and labeled as FF1, FF2, FF3, FF4, and FF5 according to the respective FA1, FA2, FA3, FA4, and FA5 as fillers. The synthesis process of the $Fe_3O_4$/Ag nanohybrid ferrofluids is shown in Figure 1.

### 2.3. Characterization

The crystal structure of the as-prepared samples was investigated using X-ray diffraction (XRD; PanAnalytical X'Pert Pro) with Cu-Kα radiation ($\lambda$ = 1.540 Å) generated at 40 kV and 15 mA; samples were scanned over the $2\theta$ range 10°–80°. The morphology of the samples was analyzed by scanning electron microscopy (SEM; FEI Inspect-S50). The surface composition of the samples was evaluated by X-ray photoelectron spectroscopy (XPS; ULVAC-PHI ESCA1600). The molecular structure of the ferrofluids was studied by Fourier transform infrared (FTIR) spectroscopy (Shimadzu IRPrestige 21) over the wavenumber range 4000–450 $cm^{-1}$. The magnetic properties were characterized by vibrating sample magnetometry (VSM; Oxford VSMI.2H). The antimicrobial activities against various bacteria (*B. subtilis*, *S. aureus*, and *E. coli*) and a fungus (*C. albicans*) were evaluated using the agar diffusion method. The *in vivo* study was approved by Institutional Review Board Universitas Brawijaya, Malang-Indonesia, with ethics certificate number 1184-KEP-UB/2019. The liver fibrosis model was designed by intraperitoneal injection of Balb-C mice strain age eight weeks old and ±25 g of BW with 100 uL $CCl_4$ solution (1 mL $CCl_4$: 3 mL corn oil). The established dosage was 1 uL/g bodyweight of each mice for 6 weeks of treatment. The experimental group was treated with the same volume of *ip*. injection with the combination of $Fe_3O_4$/Ag nanohybrid ferrofluids with serial dilutions. The blood samples were acquired from the intra-orbitalis area and stored within heparin tube collection. The samples were then analyzed for the serologic assays of the liver injury marker (ALT and AST) concentration.

## 3. Results and discussion

The XRD patterns of the $Fe_3O_4$/Ag nanocomposites FA1–FA5 are depicted in Figure 2. The phase identification showed that the $Fe_3O_4$ and Ag were formed in the spinel crystal structure and face-centered cubic, respectively. The quantitative crystal-structure analysis was carried via the Rietveld refinement method using AMCSD 0002400 for $Fe_3O_4$ and AMCSD 0013120 for Ag as the crystal structure models. The diffraction intensity of the $Fe_3O_4$ peaks, as depicted in Figure 2, is lower than that of the Ag peaks. Wang et al. attributed such a difference in peak intensity to the Ag content being greater than the $Fe_3O_4$ content [30]. However, Qi and coworkers observed very different intensities of $Fe_3O_4$ and Ag, and they attributed the difference in intensity to the Ag nanoparticles being aggregated and unevenly distributed [31]. The patterns in Figure 2 include several peaks that indicate the formation of $Fe_3O_4$ at 30.2°, 35.7°, 54.4°, and 58.0°, which are respectively indexed to the (220), (311), (422), and (511) planes of $Fe_3O_4$ [32]. However, the intensity of these peaks gradually decreases with increasing Ag content. The characteristic peaks of Ag at 38.3°, 44.3°, 64.6°, and 77.3° (corresponding to the (111), (200), (220), and (311) planes of Ag, respectively) were also observed [33]. Given the existence of the characteristic peaks of both $Fe_3O_4$ and Ag, we concluded that $Fe_3O_4$/Ag particles were successfully synthesized.

On the basis of the data analysis results, with increasing addition of Ag, the phase composition of Ag increased from 40.2% ± 6.2% (FA1) to 55.8% ± 7.6% (FA2), 59.4% ± 7.9% (FA3), 67.7% ± 7.9% (FA4), and 77.2% ± 8.4% (FA5). The crystallite size obtained by the well-known Scherrer approach from the XRD diffraction data. Our results revealed that the crystallite sizes of $Fe_3O_4$ and Ag are respectively around 11.8 ±

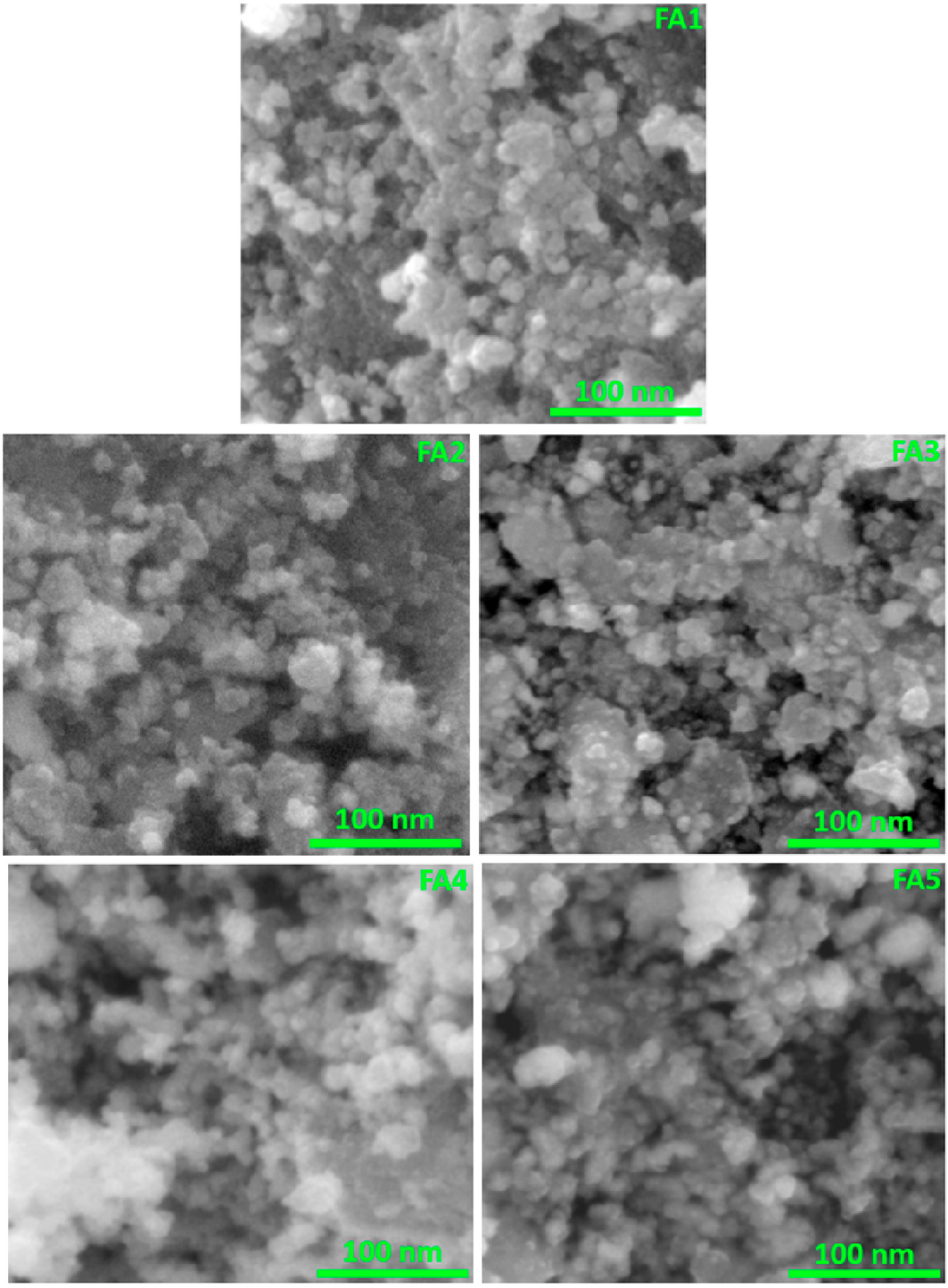


**Figure 3.** SEM micrographs of the $Fe_3O_4$/Ag nanocomposites. The samples vary by the amount of Ag added during the synthesis.

0.2–12.1 ± 0.5 nm and 36.8 ± 1.3–37.2 ± 1.8 nm. In this regard, Quynh and colleagues reported that the particle size of a $Fe_3O_4$/Ag nanocomposite increased from 15 to 50 nm with increasing Ag content [34]. In addition, the lattice parameters tended to be stable, with values of 8.344 ± 0.002 Å for $Fe_3O_4$ and 4.091 ± 0.004 Å for Ag. Thus, increasing the Ag content in the $Fe_3O_4$/Ag nanocomposites did not change the lattice parameters or the particle size.

The surface morphology of the $Fe_3O_4$/Ag nanocomposite particles was determined through SEM observations (Figure 3). The SEM micrographs show that the particles tended to agglomerate, presumably because of strong interparticle forces due to the high surface-area-to-volume ratio of the nanoparticles [35]. Consequently, primary and secondary particles tend to form relatively large particle clusters to become more stable [36].

XPS spectra of the $Fe_3O_4$/Ag nanocomposites are shown in Figure 4 to support our conjecture that the high-quality samples were synthesized. The presence of $Fe_3O_4$ was indicated by peaks at a binding energy of 711 eV, which are assigned to $Fe^{2+}$, and at binding energies of 714 eV and 727 eV, which are assigned to $Fe^{3+}$, in the Fe 2*p* XPS core-level spectra (left panel in Figure 2) [37, 38]. Interestingly, the absence of a peak characteristic of $Fe^{3+}$ ions in $Fe_2O_3$, which would appear as a satellite peak at ~719 eV, confirms that pure $Fe_3O_4$ was obtained [39]. Moreover,

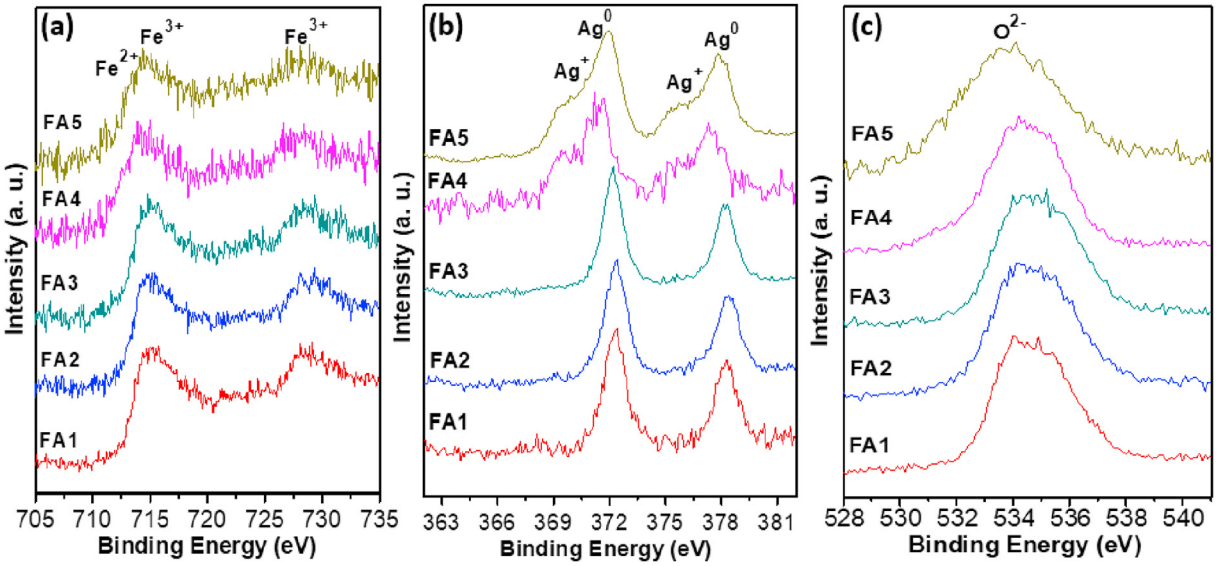


**Figure 4.** XPS spectra of the $Fe_3O_4$/Ag nanocomposites FA1–FA5: (a) Fe 2*p*, (b) Ag 3*d*, and (c) O 1*s* core-level spectra.

the presence of Ag was confirmed by the $Ag^+$ peaks at binding energies of 369 and 376 eV and $Ag^0$ peaks at binding energies of 373 and 379 eV in the Ag 3*d* XPS core-level spectra (middle panel of Figure 2) [40]. Finally, peaks representing $O^{2-}$ were observed at a binding energy of 534 eV in the O 1*s* XPS core-level spectra (right panel of Figure 2) [41].

The XPS core-level spectra of Fe 2*p*, Ag 3*d*, and O 1*s* vary with the Ag content. The signal strength of the peaks in the Fe 2*p* XPS core-level spectra decreases with increasing Ag content, which indicates that the $Fe_3O_4$ mixed well with the Ag to forms a composite nanoparticle while keeping most of the chemical composition intact. In addition, all XPS peaks have slightly shift due to the variation of Ag composition. This suggests that the interfacial surface charge distribution has changed and indicates the formation of a charge-transfer complex as well as a strong interaction between the $Fe_3O_4$ and Ag [42]. In the case of samples with a high Ag content, clear separation of the $Ag^+$ and $Ag^0$ peaks was observed in Ag 3*d* XPS core-level spectra, accompanied by a shift of the peaks in the O 1*s* XPS core-level spectra toward lower binding energies. We attribute this phenomenon to strong intermixing of the Fe and Ag ions in the samples with a high Ag content. In summary, the XPS results indicate the successful preparation of $Fe_3O_4$/Ag nanocomposites in which $Fe_3O_4$ nanoparticles interact with Ag via strong ionic bonding.

The molecular structure of $Fe_3O_4$/Ag ferrofluids was analyzed on the basis of their FTIR transmission spectra, as shown in Figure 5. The peaks of the fillers in the ferrofluids appeared at 451 and 707 $cm^{-1}$, which are associated with Fe–O bonds involving Fe ions in octahedral and tetrahedral sites, respectively [43]. Meanwhile, peaks of functional groups of Ag were detected at 1652 $cm^{-1}$ (N–Ag) and 3002 $cm^{-1}$ (C–Ag) [44]. Oleic acid as the first layer was detected by the appearance of a C=C vibration at 1312 $cm^{-1}$ [13], carboxyl group ($COO^-$) vibrations at 1401 and 1444 $cm^{-1}$ [45], and $CH_2$ vibrations at 2849 and 2910 $cm^{-1}$ [46]. In

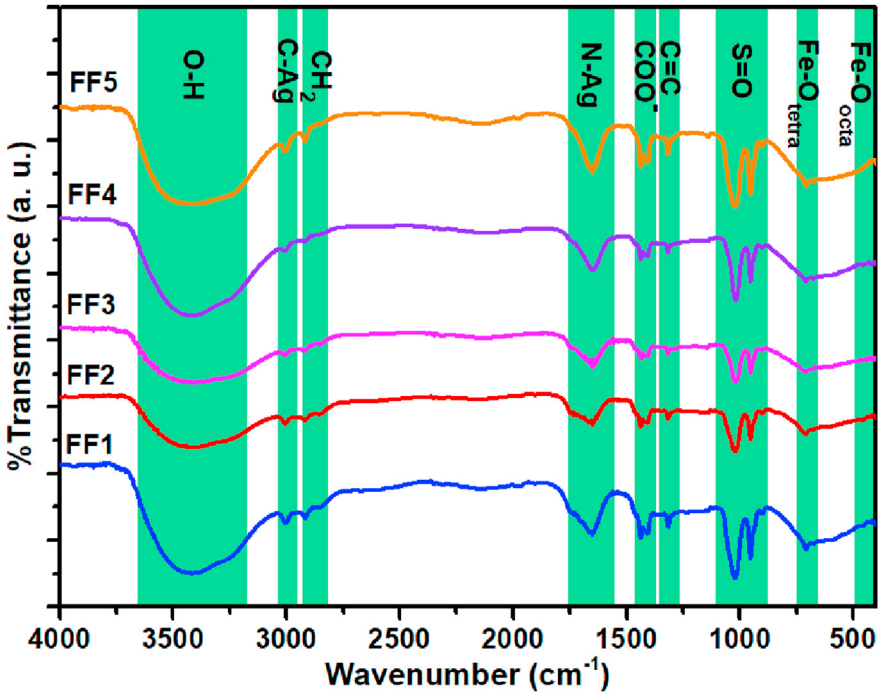


**Figure 5.** FTIR spectra of the $Fe_3O_4$/Ag ferrofluids.

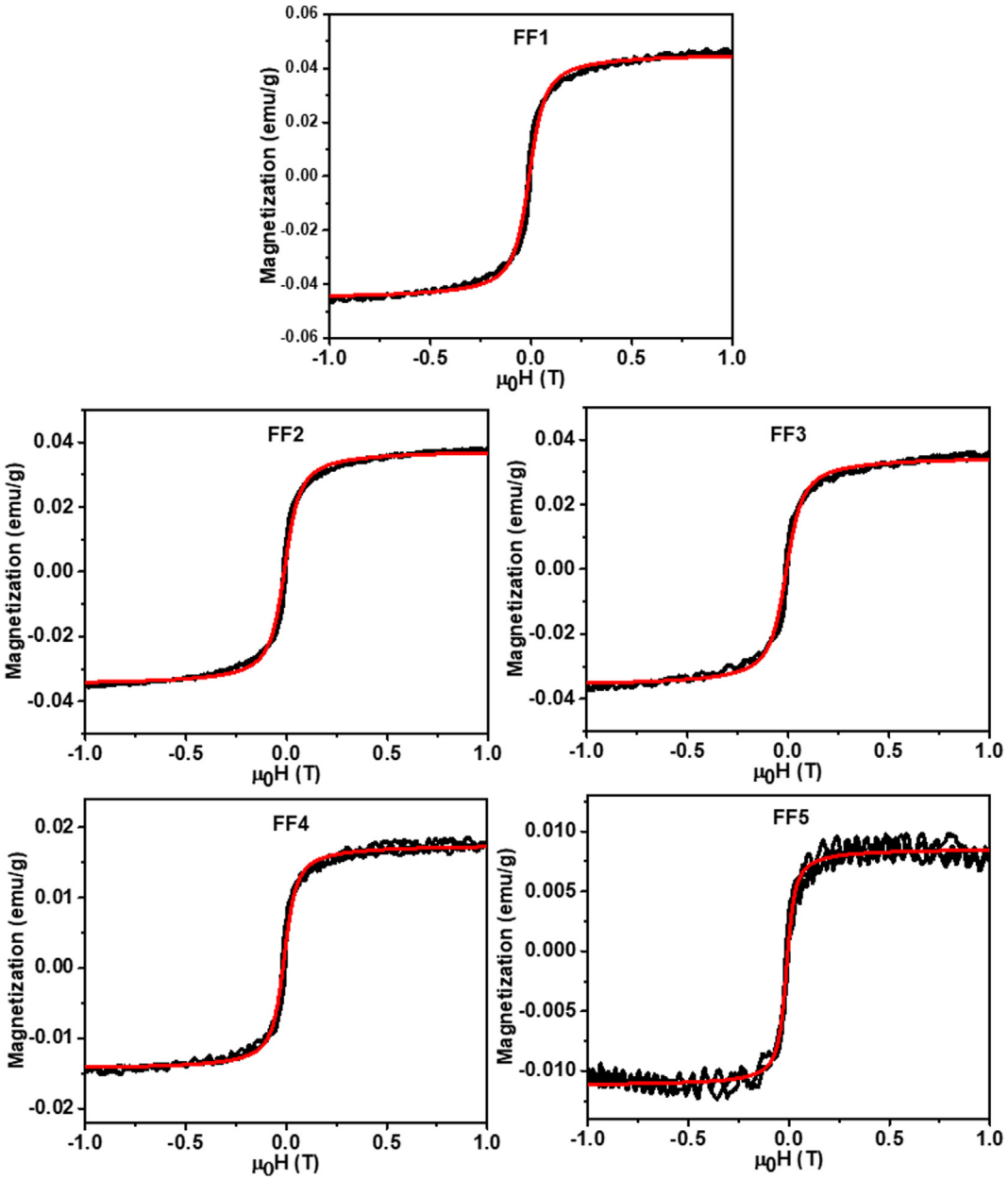


**Figure 6.** Fitted magnetization curves for the $Fe_3O_4$/Ag ferrofluids. The *black* line and *red* line represent the respective experimental data and fitting model using Langevin equation.

addition, DMSO as the second layer was detected by the appearance of peaks of S=O vibrations at 941 and 1022 $cm^{-1}$ [47]. Interestingly, the peaks of the functional groups of the olive oil used as a carrier liquid overlapped those of the functional groups of oleic acid. This observation is explained by the fact that oleic acid is the main constituent in olive oil. According to Giacintucci and colleagues, the oleic acid content of olive oil can be as high as 83% [48]. Thus, the FTIR results show that $Fe_3O_4$/Ag ferrofluids were fabricated successfully, as indicated by the identification of all of the functional groups of their components.

The magnetization curves of the $Fe_3O_4$/Ag ferrofluids and their fitting analysis are shown in Figure 6. The curves show that the as-prepared $Fe_3O_4$/Ag ferrofluids exhibit superparamagnetic character, as indicated by the hysteresis curves, which resemble the letter "S" and have a very small coercivity field [49]. Furthermore, when compared with the hysteresis curves of magnetic samples in general, the curves obtained in the present study are less smooth. This lack of smoothness is attributed to all of the components of the ferrofluid, including the surfactants and dispersants, vibrating when the samples are measured by VSM. Consequently, the surfactants and dispersants, which are nonmagnetic materials, contribute to the instability of the curve, resulting in a hysteresis curve that is not smooth. The fitting analysis was performed by using the Langevin equation, as shown in Eq. (1) [50]:

$$M = M_s\left(\coth\left(\frac{\mu H}{k_B T}\right) - \left(\frac{k_B T}{\mu H}\right)\right) \quad (1)$$

where $M$ is the magnetization, $M_s$ is the saturation magnetization, $\mu$ is the magnetic moment, $H$ is the magnetic field (T), $k_B$ is the Boltzmann constant, and $T$ is the temperature. In general, the Langevin equation (solid red lines in Figure 6) well fit the magnetization data (solid black lines).

The data analysis results show that the saturation magnetization of the $Fe_3O_4$/Ag ferrofluids decreased from $0.046 \pm 0.007$ to $0.010 \pm 0.002$ emu/g with increasing Ag content, which is a nonmagnetic material. A similar decrease was observed for the material coercivity field. Tung and

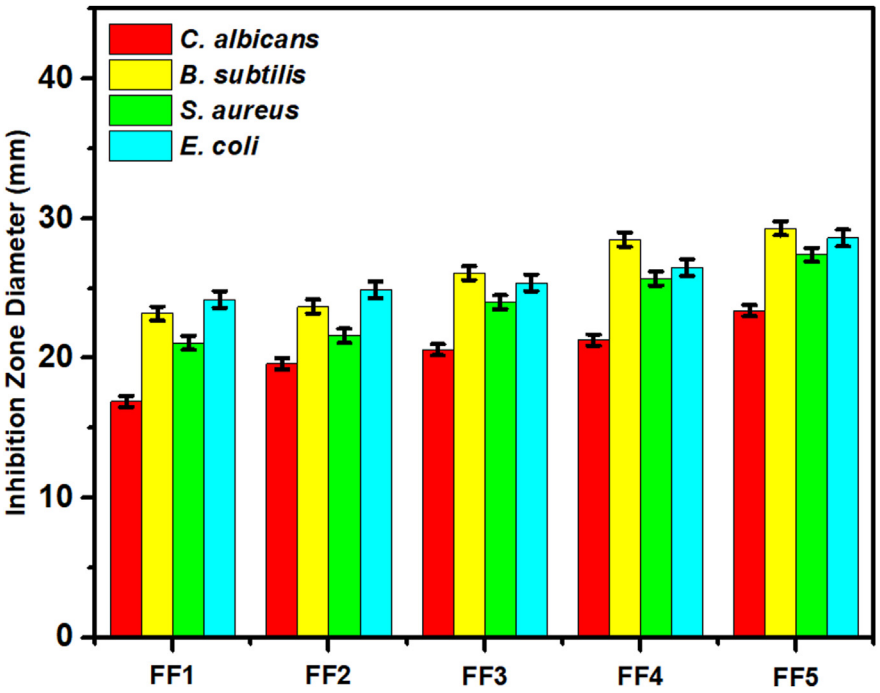


**Figure 7.** Inhibition zone diameter of the $Fe_3O_4$/Ag ferrofluids against fungus *C. albicans* and bacteria *B. subtilis*, *S. aureus*, and *E. coli*.

coworkers reported similar results, where the saturation magnetization decreased from 55.35 to 52.98 emu/g [14], accompanied by a decrease in the coercivity field, which decreased from 0.0027 ± 0.0007 to 0.0011 ± 0.0002 T as well as the remanence which decreased from 0.037 ± 0.006 to 0.010 ± 0.002 emu/g. The decrease in saturation magnetization results in a decrease in the magnetic moment of the material, where the material becomes more quickly oriented with an external magnetic field. The saturation magnetization of the ferrofluids was very small–substantially smaller than that of $Fe_3O_4$ bulk (~90 emu/g) [51]. Other previously reported saturation magnetization values include 50.53 emu/g for $Fe_3O_4$/Ag microspheres [52] and 64 emu/g for $Fe_3O_4$/Ag nanocomposites [53].

The antimicrobial activity of the $Fe_3O_4$/Ag ferrofluids against fungus *C. albicans* and bacteria *B. subtilis*, *S. aureus*, and *E. coli* was investigated

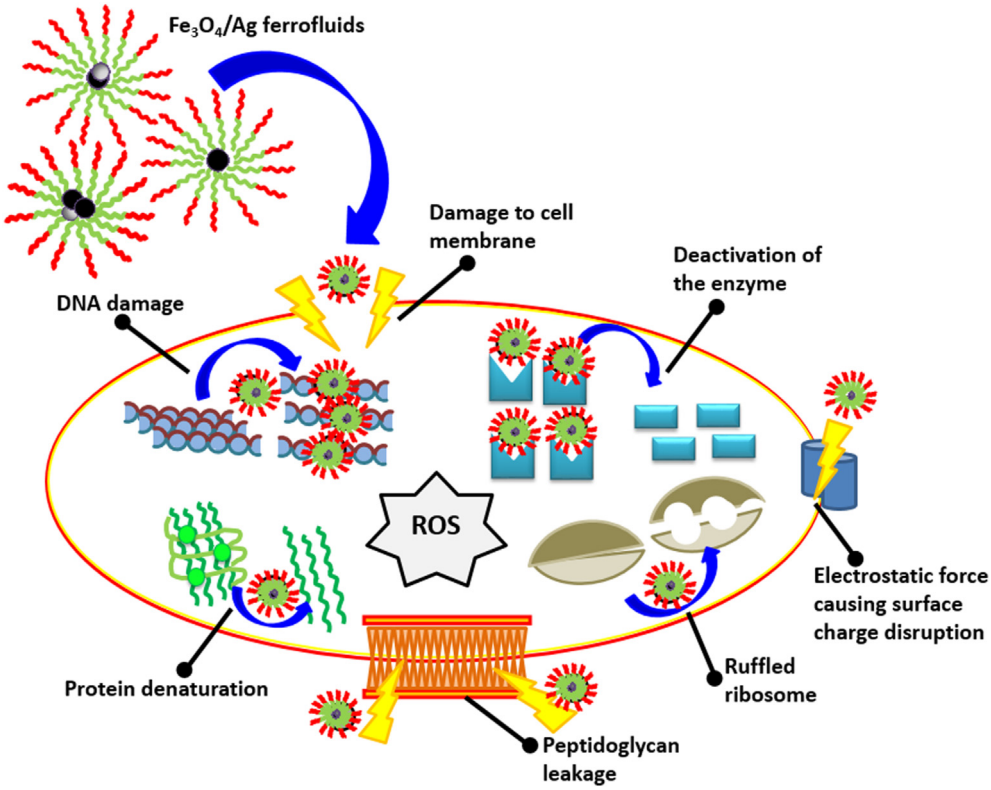


**Figure 8.** Mechanism of bacterial destruction by the $Fe_3O_4$/Ag ferrofluids.

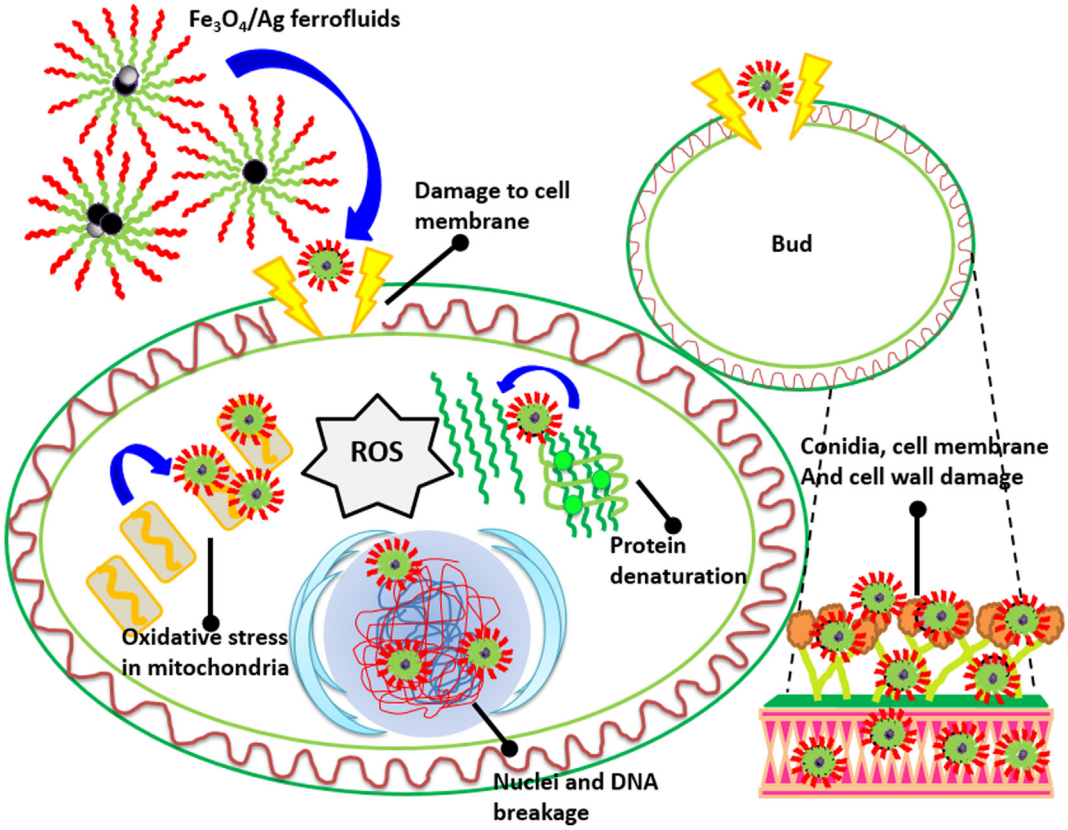


**Figure 9.** Mechanism of fungal destruction by the $Fe_3O_4$/Ag ferrofluids.

by the agar diffusion method, as shown in Figure 7. With increasing Ag content, the diameter of the inhibition zone of the $Fe_3O_4$/Ag ferrofluids increased, indicating an increase in antimicrobial performance. The results indicate that increasing Ag content plays an essential role in disrupting microbial growth. Tung et al. explained that not only $Fe^{2+}$ and $Fe^{3+}$ but also $Ag^{+}$ are released, generating positively charged $Fe_3O_4$/Ag [14]. Furthermore, the electrostatic attraction between microbial cell walls and $Fe_3O_4$/Ag increases because the microbial cell walls are negatively charged, leading to a large density of $Fe_3O_4$/Ag attached to the surface of the cell membrane. The nanometric dimensions of the particles enhance their specific surface area, enabling a large contact area between the $Fe_3O_4$/Ag and the microbial cell membranes. Ye and coworkers explained that nanoparticles more easily penetrate microbial pores [54]. Interestingly, in the ferrofluid system, the $Fe_3O_4$/Ag more easily disrupts cellular construction, resulting in cell death because ferrofluids more easily dissolve the outer envelope of the microbial cell walls. Furthermore, reactive oxygen species (ROS) contained in metal oxides release and attack the microbial nucleus and pathogenic DNA [55].

In the present study, the use of ferrofluids contributed to superior antimicrobial performance. The proposed mechanisms of destruction of the bacteria and fungus are presented in Figures 8 and 9; the antibacterial mechanism is based on that of Roy et al. [56], and the antifungal mechanism is based on that of Rai et al. [57]. Theoretically, the surface charge of nanoparticles containing ROS in the form of superoxide ions surrounded by surfactants becomes positive. By contrast, the charge around the surface of microbes is negative, which results in electrostatic attraction between the nanoparticles and microbes. Furthermore, ROS produced by fillers in ferrofluids easily enter microbial pores, thereby enhancing destruction of the microbial cell nucleus and pathogenic DNA. The antimicrobial ability of the samples was supported by the disinfecting capability of the Ag nanoparticles [58]. In a complex process, the antimicrobial activity of the $Fe_3O_4$/Ag ferrofluids and their ions caused the release of $Fe^{2+}$, $Fe^{3+}$, and $Ag^{+}$ ions, which generated free radicals that subsequently induced oxidative stress associated with the presence of ROS.

Determining whether the $Fe_3O_4$/Ag ferrofluids are more effective as antimicrobial agents than $Fe_3O_4$/Ag powders is important. Taghizadeh et al. reported that $Fe_3O_4$/Ag nanopowders exhibited inhibition zone diameters of approximately 8–10 mm against *S. aureus* and 9–10 mm against *E. coli* [59]. In a similar study, Yong and coworkers showed that nanocomposites of $Fe_3O_4$/Ag coated with ethylenediamine chitosan/polyacrylic acid exhibited inhibition zone diameters of 8.4 mm against *E. coli* and 9.6 mm against *S. aureus*. Furthermore, Hassiba et al., who successfully modified Ag nanoparticles with various polymers, reported an inhibition zone diameter of approximately 16 mm against both *E. coli* and *S. aureus* [60].

The baseline characteristics of serum liver injury marker showed in Figure 10 and Figure 11. Fascinatingly, the application of $Fe_3O_4$/Ag ferrofluids with a serial dilution of magnetic and silver nanoparticles significantly decreases the circulating level of ALT and AST compared to $CCl_4$ groups. The feature of this ferrofluids exposure linear to the placebo

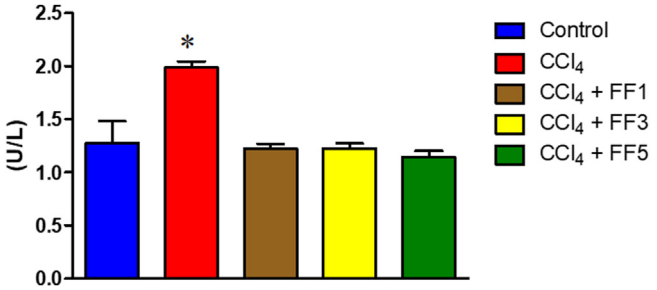


**Figure 10.** Plasma level of Alanine Aminotransferase (ALT) after $CCl_4$treatment. *Significant different vs control group with p-value $< 0.05$.

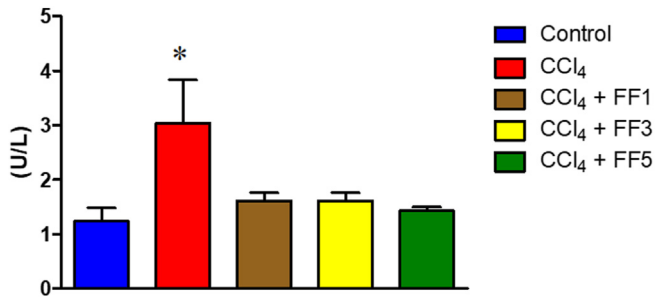


**Figure 11.** Plasma level of Aspartate Aminotransferase (AST) after $CCl_4$ treatment. *Significant different vs control group with p-value < 0.05.

contributor to liver fibrosis is HSCs [64]. Hence, these cells play a pivotal role in the pathogenesis of liver fibrosis. The development of liver fibrosis management is strongly supported by magnetic nanoparticles-based therapy [65, 66, 67]. Currently, most liver fibrosis treatment is based on iron oxide nanoparticles [68]. Besides, the hybrid nanoparticles can also be applied for liver fibrosis diagnosis and treatment. However, the limitation of our in vivo study remains. The baseline data of animal model pre-treated by $CCl_4$ and $Fe_3O_4$/Ag ferrofluids cannot provide complete information-associated histological changes. The alteration of liver structure and ECM accumulation should be confirmed as the supporting data to ensure that these ferrofluids potential as nanodrugs candidate against liver fibrosis. Also, the molecular mechanism on how ferrofluids can inhibit the progression of liver fibrosis is not fully eluci-

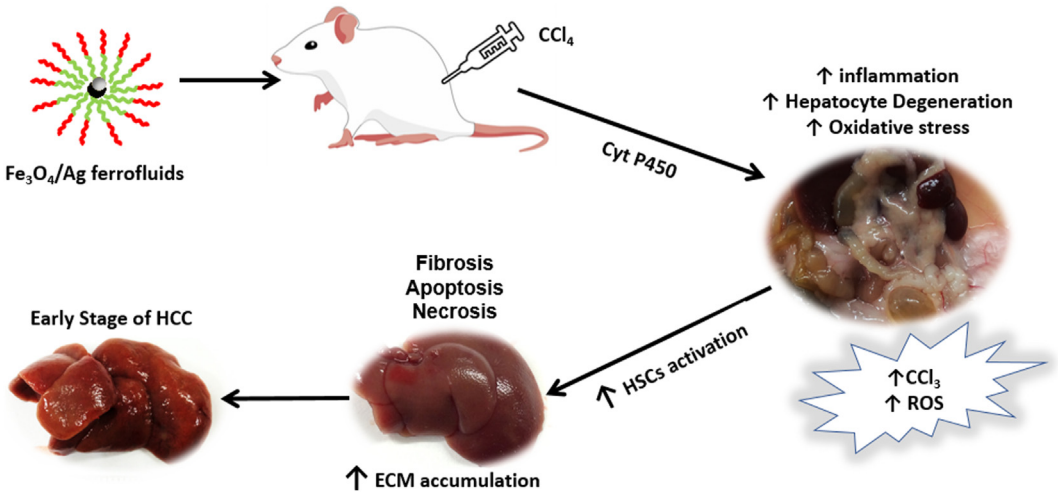


**Figure 12.** The hypothetical framework of the $Fe_3O_4$/Ag ferrofluids activity in liver fibrosis development.

data in which the combination treatment of $CCl_4$ and the ferrofluids reduced the elevating levels of ALT and AST. This data implies that the application of the ferrofluids can prevent the gradual changes of physiological stress within the parenchymal cells of the liver. However, the underlying of this mechanism still not fully elucidated. The underlying mechanism on how $CCl_4$ induce liver fibrosis has shown in Figure 12. Pre-treatment of the animal model with $CCl_4$ will trigger the liver injury-related chronic inflammation. $CCl_4$ within the liver organ will be metabolized into the new reactive form $CCl_3$ by cytochrome P450. As a result, the production of reactive oxygen species significantly increased results in a higher level of pro-inflammatory cytokine release and oxidative stress. In line with the higher level of ROS and pro-inflammatory cytokine, the hepatocyte progress to apoptosis while the activation of HSCs enhanced an excess ECM. Thus, the liver has developed to severe fibrosis, steatosis, and showed as in irregular shape.

In general, the application of $Fe_3O_4$/Ag ferrofluids significantly reduces the level of ALT and AST in our liver fibrosis model. We hypothesized that the combination treatment of $CCl_4$ and $Fe_3O_4$/Ag ferrofluids could decrease the progression of liver fibrosis-related inflammation and fibrogenic activity on hepatic stellate cells (HSCs). Importantly, deregulated inflammation is the primary target of liver fibrosis prevention. Liver fibrosis was established as the first enhancer in the early stage of hepatocellular carcinoma development. The chronic inflammation incidence within the liver leads to improve extracellular matrix (ECM) remodeling progress to severe fibrosis [61]. The activation of pro-inflammatory cells and HSCs will trigger liver failure. The excessive ECM induces liver stiffness and may affect another organ in the body.

Nowadays, the clinical and translational investigation is addressed to a novel invention for liver fibrosis treatment. The investigator tried to focus on reducing inflammation dan develop new drugs that effectively regulate connective tissue in the liver [62, 63]. Interestingly, the primary dated. Therefore, further study could be addressed to this related issue to fully understood the primary contribution of ferrofluids to liver fibrosis-HCC development.

## 4. Conclusions

Double-layered $Fe_3O_4$/Ag nanohybrid ferrofluids were fabricated using a simple synthesis approach. All of the samples exhibited pure phases of $Fe_3O_4$ and Ag without impurities and exhibited stable crystallite sizes of 11.8–12.1 nm for $Fe_3O_4$ and 36.8–37.2 nm for Ag. The crystallite phase increased from 40.2% to 77.2% with increasing Ag content. XPS results indicated strong ionic interaction between $Fe_3O_4$ and Ag. Moreover, the XPS results suggested that the $Fe_3O_4$ mixed well with the Ag to forms a composite nanoparticle while keeping most of the chemical composition intact. The existence of $Fe_3O_4$/Ag, oleic acid, and DMSO as the filler, first layer, and second layer was detected by FTIR. The saturation magnetization of the $Fe_3O_4$/Ag nanohybrid ferrofluids decreased with decreasing Ag content and indicated superparamagnetic behavior. Interestingly, the as-prepared $Fe_3O_4$/Ag nanohybrid ferrofluids demonstrated excellent antimicrobial performance. The prepared $Fe_3O_4$/Ag ferrofluids significantly reduced the level of ALT and AST in the liver fibrosis model and decreased the progression of liver fibrosis-related inflammation and fibrogenic activity on hepatic stellate cells.

## Declarations

### *Author contribution statement*

Ahmad Taufiq: Conceived and designed the experiments; Analyzed and interpreted the data; Wrote the paper.

Rosy Eko Saputro, Nurul Hidayat: Performed the experiments; Wrote the paper.

Hendra Susanto, Sunaryono Sunaryono, Tahta Amrillah: Performed the experiments; Analyzed and interpreted the data.

Husni Wahyu Wijaya, Nandang Mufti, Firman Mangasa Simanjuntak: Analyzed and interpreted the data; Contributed reagents, materials, analysis tools or data.

## Funding statement

This work was supported by Universitas Negeri Malang (10.3.63/UN32.14.1/LT/2020).

## Data availability statement

Data will be made available on request.

## Declaration of interests statement

The authors declare no conflict of interest.

## Additional information

No additional information is available for this paper.

## References

[1] B. Yih Hui, N.N. Mohamad Zain, S. Mohamad, P. Varanusupakul, H. Osman, M. Raoov, Poly(cyclodextrin-ionic liquid) based ferrofluid: a new class of magnetic colloid for dispersive liquid phase microextraction of polycyclic aromatic hydrocarbons from food samples prior to GC-FID analysis, Food Chem. 314 (2020) 126214.

[2] X. Zhang, L. Sun, Y. Yu, Y. Zhao, Flexible ferrofluids: design and applications, Adv. Mater. 31 (2019) 1903497.

[3] T.K. Oanh Vuong, T.T. Le, H.D. Do, X.T. Nguyen, X.C. Nguyen, T.T. Vu, T.L. Le, D.L. Tran, PMAO-assisted thermal decomposition synthesis of high-stability ferrofluid based on magnetite nanoparticles for hyperthermia and MRI applications, Mater. Chem. Phys. 245 (2020) 122762.

[4] A. Taufiq, F.N. Ikasari, N. Hidayat, H.N. Ulya, R.E. Saputro, N. Mufti, A. Hidayat, S. Sunaryono, L. Chuenchom, Dependence of PEO content in the preparation of $Fe_3O_4$/PEO/TMAH ferrofluids and their antibacterial activity, J. Polym. Res. 27 (2020) 117.

[5] L. de, A.S. de Toledo, H.C. Rosseto, R.S. dos Santos, F. Spizzo, L. Del Bianco, M.C. Montanha, E. Esposito, E. Kimura, P. de Souza Bonfim-Mendonça, T.I.E. Svidzinski, Thermal magnetic field activated propolis release from liquid crystalline system based on magnetic nanoparticles, AAPS PharmSciTech 19 (2018) 3258–3271.

[6] H.Y. Zhao, S. Liu, J. He, C.C. Pan, H. Li, Z.Y. Zhou, Y. Ding, D. Huo, Y. Hu, Synthesis and application of strawberry-like $Fe_3O_4$-Au nanoparticles as CT-MR dual-modality contrast agents in accurate detection of the progressive liver disease, Biomaterials 51 (2015) 194–207.

[7] Z. Jiang, K. Shan, J. Song, J. Liu, S. Rajendran, A. Pugazhendhi, J.A. Jacob, B. Chen, Toxic effects of magnetic nanoparticles on normal cells and organs, Life Sci. 220 (2019) 156–161.

[8] Y. Li, A.R. Zimmerman, F. He, J. Chen, L. Han, H. Chen, X. Hu, B. Gao, Solvent-free synthesis of magnetic biochar and activated carbon through ball-mill extrusion with $Fe_3O_4$ nanoparticles for enhancing adsorption of methylene blue, Sci. Total Environ. 722 (2020) 137972.

[9] M. Sakaguchi, M. Makino, T. Ohura, K. Yamamoto, Y. Enomoto, H. Takase, Surface modification of $Fe_3O_4$ nanoparticles with dextran via a coupling reaction between naked $Fe_3O_4$ mechano-cation and naked dextran mechano-anion: a new mechanism of covalent bond formation, Adv. Powder Technol. 30 (2019) 795–806.

[10] M. Bahiraei, M. Hangi, A. Rahbari, A two-phase simulation of convective heat transfer characteristics of water–$Fe_3O_4$ ferrofluid in a square channel under the effect of permanent magnet, Appl. Therm. Eng. 147 (2019) 991–997.

[11] X. Wang, A. Cai, X. Wen, D. Jing, H. Qi, H. Yuan, Graphene oxide-$Fe_3O_4$ nanocomposites as high-performance antifungal agents against Plasmopara viticola, Sci. China Mater. 60 (2017) 258–268.

[12] S.M. Ghaseminezhad, S.A. Shojaosadati, Evaluation of the antibacterial activity of Ag/$Fe_3O_4$ nanocomposites synthesized using starch, Carbohydr. Polym. 144 (2016) 454–463.

[13] A. Taufiq, R.E. Saputro, Y.A. Hariyanto, N. Hidayat, A. Hidayat, N. Mufti, H. Susanto, Functional group and magnetic properties of $Fe_3O_4$ ferrofluids: the impact of dispersion agent composition, in: Journal of Physics: Conference Series, IOP Publishing, 2018, 012010.

[14] L.M. Tung, N.X. Cong, L.T. Huy, N.T. Lan, V.N. Phan, N.Q. Hoa, L.K. Vinh, N.V. Thinh, L.T. Tai, D.-T. Ngo, K. Mølhave, T.Q. Huy, A.-T. Le, Synthesis, characterizations of superparamagnetic $Fe_3O_4$–Ag hybrid nanoparticles and their application for highly effective bacteria inactivation, J. Nanosci. Nanotechnol. 16 (2016) 5902–5912.

[15] R. Sharifi, A.H. Hassani, H. Ahmad Panahi, M. Borghei, Performance of silver nanoparticle fixed on magnetic iron nanoparticles ($Fe_3O_4$-Ag- $Fe_3O_4$−Ag) in water disinfection, Micro & Nano Lett. 13 (2018) 436–441.

[16] V.T. Trang, N. Van Quy, T.Q. Huy, N.T. Thuy, D.Q. Tri, N.D. Cuong, P.A. Tuan, H. Van Tuan, A.-T. Le, V.N. Phan, Functional iron oxide–silver hetero-nanocomposites: controlled synthesis and antibacterial activity, J. Electron. Mater. 46 (2017) 3381–3389.

[17] R.E. Saputro, A. Taufiq, Sunaryono, N. Hidayat, A. Hidayat, Effects of DMSO content on the optical properties, liquid stability, and antimicrobial activity of $Fe_3O_4$/OA/DMSO ferrofluids, Nano 15 (2020) 2050067.

[18] M. Latikka, M. Backholm, J.V.I. Timonen, R.H.A. Ras, Wetting of ferrofluids: phenomena and control, Curr. Opin. Colloid Interface Sci. 36 (2018) 118–129.

[19] H. Cui, D. Li, Fabrication and properties research on a novel perfluoropolyether based ferrofluid, J. Magn. Magn Mater. 473 (2019) 341–347.

[20] R. Singh, G. Thirupathi, Manganese-zinc spinel ferrite nanoparticles and ferrofluids, in: Magnetic Spinels-Synthesis, Properties and Applications, InTech, 2017.

[21] S.M. Hosseini, L. Vafajoo, E. Ghasemi, B.H. Salman, Experimental investigation the effect of nanoparticle concentration on the rheological behavior of paraffin-based nickel ferrofluid, Int. J. Heat Mass Tran. 93 (2016) 228–234.

[22] J. Kurimský, M. Rajňák, P. Bartko, K. Paulovičová, R. Cimbala, D. Medveď, M. Džamová, M. Timko, P. Kopčanský, Experimental study of AC breakdown strength in ferrofluid during thermal aging, J. Magn. Magn Mater. 465 (2018) 136–142.

[23] K. Zipare, J. Dhumal, S. Bandgar, V. Mathe, G. Shahane, Superparamagnetic manganese ferrite nanoparticles: synthesis and magnetic properties, J. Nanosci. Nanoeng. 1 (2015) 178–182.

[24] C. Zhang, H. Liu, Y. Cui, X. Li, Z. Zhang, Y. Zhang, D. Wang, Molecular magnetic resonance imaging of activated hepatic stellate cells with ultrasmall superparamagnetic iron oxide targeting integrin $\alpha v\beta_3$ for staging liver fibrosis in rat model, Int. J. Nanomed. 11 (2016) 1097–1108.

[25] Z. Kong, R. Liu, Y. Cheng, Artesunate alleviates liver fibrosis by regulating ferroptosis signaling pathway, Biomed. Pharmacother. 109 (2019) 2043–2053.

[26] M. Dodson, R. Castro-Portuguez, D.D. Zhang, NRF2 plays a critical role in mitigating lipid peroxidation and ferroptosis, Redox Biol. 23 (2019) 101107.

[27] L.H. Reddy, P. Couvreur, Nanotechnology for therapy and imaging of liver diseases, J. Hepatol. 55 (2011) 1461–1466.

[28] M. Imran, A.R. Ansari, A.H. Shaik, S. Hussain, A. Khan, M.R. Chandan, Ferrofluid synthesis using oleic acid coated $Fe_3O_4$ nanoparticles dispersed in mineral oil for heat transfer applications, Mater. Res. Express 5 (2018), 036108.

[29] G.M. Madruga, L.Z. Crivellenti, S. Borin-Crivellenti, C.A. Cintra, L.G. Gomes, P.R. Spiller, Comparative use of dimethyl sulphoxide (DMSO) in different animal species, Vet. Med. 62 (2017) 179–185.

[30] J. Wang, X. Yang, A. Li, X. Cai, Preparation and characterization of multifunctional $Fe_3O_4$-coated Ag nanocomposites for catalytic reduction of 4-nitrophenol, Mater. Lett. 220 (2018) 24–27.

[31] C.-C. Qi, J.-B. Zheng, Synthesis of $Fe_3O_4$–Ag nanocomposites and their application to enzymeless hydrogen peroxide detection, Chem. Pap. 70 (2016) 404–411.

[32] A. Taufiq, N. Wahyuni, R.E. Saputro, N. Mufti, Sunaryono, A. Hidayat, D. Yuliantika, N. Hidayat, Mujamilah, Investigation of structural, magnetic and antibacterial activities of $Cr_xFe_{3-x}O_4$ ferrofluids, Mol. Cryst. Liq. Cryst. 694 (2019) 60–72.

[33] B.A. Fahimmunisha, R. Ishwarya, M.S. AlSalhi, S. Devanesan, M. Govindarajan, B. Vaseeharan, Green fabrication, characterization and antibacterial potential of zinc oxide nanoparticles using Aloe socotrina leaf extract: a novel drug delivery approach, J. Drug Deliv. Sci. Technol. 55 (2020) 101465.

[34] L.M. Quynh, C.T. Dung, B.T. Mai, H.V. Huy, N.Q. Loc, N.Q. Hoa, P.T. Thach, B.V. Anh, C.T. Thao, N.H. Nam, Development of $Fe_3O_4$/Ag core/shell-based multifunctional immunomagnetic nanoparticles for isolation and detection of CD34 + stem cells, J. Immunoassay Immunochem. 39 (2018) 308–322.

[35] Z. Wang, J. Huang, W. Huang, H. Yamamoto, S. Kawaguchi, M. Nagai, Agglomeration controllable reprecipitation method using solvent mixture for synthesizing conductive polymer nanoparticles, Colloid Polym. Sci. 297 (2019) 69–76.

[36] Sunaryono, A. Taufiq, E.G.R. Putra, A. Okazawa, I. Watanabe, N. Kojima, S. Rugmai, S. Soontaranon, M. Zainuri, Triwikantoro, Small-angle X-ray scattering study on PVA/$Fe_3O_4$ magnetic hydrogels, Nano 11 (2016) 1650027.

[37] T. Radu, A. Petran, D. Olteanu, I. Baldea, M. Potara, R. Turcu, Evaluation of physico-chemical properties and biocompatibility of new surface functionalized $Fe_3O_4$ clusters of nanoparticles, Appl. Surf. Sci. 501 (2020) 144267.

[38] D. Tahir, S. Ilyas, B. Abdullah, B. Armynah, H.J. Kang, Electronic properties of composite iron (II, III) oxide ($Fe_3O_4$) carbonaceous absorber materials by electron spectroscopy, J. Electron. Spectrosc. Relat. Phenom. 229 (2018) 47–51.

[39] Y. Li, Z. Wang, Z. Ali, K. Tian, J. Xu, W. Li, Y. Hou, Monodisperse $Fe_3O_4$ spheres: large-scale controlled synthesis in the absence of surfactants and chemical kinetic process, Sci. China Mater. 62 (2019) 1488–1495.

[40] K. Yasuda, N. Tanaka, N. Wada, H. Nishimura, Creation and functional control of metal nanoparticle-polymer interface by laser plasma EUV light excitation, in: 2018 International Conference on Electronics Packaging and IMAPS All Asia Conference (ICEP-IAAC), IEEE, 2018, pp. 535–538.

[41] R. Madhuvilakku, S. Alagar, R. Mariappan, S. Piraman, Green one-pot synthesis of flowers-like $Fe_3O_4$/rGO hybrid nanocomposites for effective electrochemical detection of riboflavin and low-cost supercapacitor applications, Sensor. Actuator. B Chem. 253 (2017) 879–892.

[42] L. Chen, H. Sun, Y. Zhao, Y. Zhang, Y. Wang, Y. Liu, X. Zhang, Y. Jiang, Z. Hua, J. Yang, Plasmonic-induced SERS enhancement of shell-dependent Ag@$Cu_2O$ core–shell nanoparticles, RSC Adv. 7 (2017) 16553–16560.
[43] A. Gholizadeh, A comparative study of physical properties in $Fe_3O_4$ nanoparticles prepared by coprecipitation and citrate methods, J. Am. Ceram. Soc. 100 (2017) 3577–3588.
[44] M. Diantoro, D. Pradhana, A.A. Mustikasari, A.D. Kusumawati, A. Taufiq, N. Mufti, H. Nur, Effect of $Fe_3O_4$ on the electro-optic and magneto-electric characteristics of (PANI/$Fe_3O_4$)-Ag film, in: IOP Conference Series: Materials Science and Engineering, IOP Publishing, 2017, 012062.
[45] M.S. Darwish, Effect of carriers on heating efficiency of oleic acid-stabilized magnetite nanoparticles, J. Mol. Liq. 231 (2017) 80–85.
[46] N.C.C. Lobato, Â. de Mello Ferreira, M.B. Mansur, Evaluation of magnetic nanoparticles coated by oleic acid applied to solvent extraction processes, Separ. Purif. Technol. 168 (2016) 93–100.
[47] R.E. Saputro, A. Taufiq, N. Hidayat, Y.A. Hariyanto, A. Hidayat, Preparation of $Fe_3O_4$/OA/DMSO ferrofluids using a double surfactant system as antifungal materials candidate, in: IOP Conference Series: Materials Science and Engineering, IOP Publishing, 2019, 012029.
[48] V. Giacintucci, C. Di Mattia, G. Sacchetti, L. Neri, P. Pittia, Role of olive oil phenolics in physical properties and stability of mayonnaise-like emulsions, Food Chem. 213 (2016) 369–377.
[49] B. Dhanalakshmi, K.V. Vivekananda, B.P. Rao, P.S.V.S. Rao, Superparamagnetism in $Bi_{0.95}Mn_{0.05}FeO_3$–$Ni_{0.5}Zn_{0.5}Fe_2O_4$ multiferroic nanocomposites, Phys. B Condens. Matter 571 (2019) 5–9.
[50] G. Drachuck, Z. Salman, M.W. Masters, V. Taufour, T.N. Lamichhane, Q. Lin, W.E. Straszheim, S.L. Bud'Ko, P.C. Canfield, Effect of nickel substitution on magnetism in the layered van der Waals ferromagnet $Fe_3GeTe_2$, Phys. Rev. B 98 (2018) 144434.
[51] C.-C. Fu, H.N. Tran, X.-H. Chen, R.-S. Juang, Preparation of polyaminated $Fe_3O_4$@chitosan core-shell magnetic nanoparticles for efficient adsorption of phosphate in aqueous solutions, J. Ind. Eng. Chem. 83 (2020) 235–246.
[52] Y. Xing, X.-H. Bai, Y. Gong, M.-L. Peng, Y.-Y. Zhang, X.-R. Ma, Y. Zhang, Enhanced catalytic properties of $Fe_3O_4$/Ag magnetic microspheres synthesized by a novel thermal co-reduction method, J. Magn. Magn Mater. 510 (2020) 166951.
[53] Y. Xing, F.-F. Ma, M.-L. Peng, X.-R. Ma, Y. Zhang, Y.-L. Cui, Bifunctional sodium tartrate as stabilizer and reductant for the facile synthesis of $Fe_3O_4$/Ag nanocomposites with catalytic activity, J. Magn. Magn Mater. 471 (2019) 133–141.
[54] W. Ye, T. Chen, Y. Mao, F. Tian, P. Sun, M. Yang, The effect of pore size in an ultrasensitive DNA sandwich-hybridization assay for the Escherichia coli O157: H7 gene based on the use of a nanoporous alumina membrane, Microchim. Acta 184 (2017) 4835–4844.
[55] Y.T. Prabhu, K.V. Rao, B.S. Kumari, V.S.S. Kumar, T. Pavani, Synthesis of $Fe_3O_4$ nanoparticles and its antibacterial application, Int. Nano Lett. 5 (2015) 85–92.
[56] A. Roy, O. Bulut, S. Some, A.K. Mandal, M.D. Yilmaz, Green synthesis of silver nanoparticles: biomolecule-nanoparticle organizations targeting antimicrobial activity, RSC Adv. 9 (2019) 2673–2702.
[57] M. Rai, A.P. Ingle, P. Paralikar, N. Anasane, R. Gade, P. Ingle, Effective management of soft rot of ginger caused by Pythium spp. and Fusarium spp.: emerging role of nanotechnology, Appl. Microbiol. Biotechnol. 102 (2018) 6827–6839.
[58] Z. Qiao, Y. Yao, S. Song, M. Yin, J. Luo, Silver nanoparticles with pH induced surface charge switchable properties for antibacterial and antibiofilm applications, J. Mater. Chem. B 7 (2019) 830–840.
[59] S.-M. Taghizadeh, A. Berenjian, S. Taghizadeh, Y. Ghasemi, A. Taherpour, A.K. Sarmah, A. Ebrahiminezhad, One-put green synthesis of multifunctional silver iron core-shell nanostructure with antimicrobial and catalytic properties, Ind. Crop. Prod. 130 (2019) 230–236.
[60] A.J. Hassiba, M.E. El Zowalaty, T.J. Webster, A.M. Abdullah, G.K. Nasrallah, K.A. Khalil, A.S. Luyt, A.A. Elzatahry, Synthesis, characterization, and antimicrobial properties of novel double layer nanocomposite electrospun fibers for wound dressing applications, Int. J. Nanomed. 12 (2017) 2205.
[61] J.K. Tee, F. Peng, H.K. Ho, Effects of inorganic nanoparticles on liver fibrosis: optimizing a double-edged sword for therapeutics, Biochem. Pharmacol. 160 (2019) 24–33.
[62] J. Ribera, J. Rodríguez-Vita, B. Cordoba, I. Portolés, G. Casals, E. Casals, W. Jiménez, V. Puntes, M. Morales-Ruiz, Functionalized cerium oxide nanoparticles mitigate the oxidative stress and pro-inflammatory activity associated to the portal vein endothelium of cirrhotic rats, PloS One 14 (2019), e0218716.
[63] C. Janko, T. Ratschker, K. Nguyen, L. Zschiesche, R. Tietze, S. Lyer, C. Alexiou, Functionalized superparamagnetic iron oxide nanoparticles (SPIONs) as platform for the targeted multimodal tumor therapy, Front. Oncol. 9 (2019) 1–9.
[64] E. Devaraj, S. Rajeshkumar, Nanomedicine for hepatic fibrosis, in: A.K. Shukla (Ed.), Nanoparticles and Their Biomedical Applications, Springer, Singapore, 2020, pp. 45–64.
[65] S. Poilil Surendran, R. George Thomas, M.J. Moon, Y.Y. Jeong, Nanoparticles for the treatment of liver fibrosis, Int. J. Nanomed. 12 (2017) 6997–7006.
[66] Q. Zhang, D. Xu, Q. Guo, W. Shan, J. Yang, T. Lin, S. Ye, X. Zhou, Y. Ge, S. Bi, L. Ren, Theranostic quercetin nanoparticle for treatment of hepatic fibrosis, Bioconjugate Chem. 30 (2019) 2939–2946.
[67] D. Oró, T. Yudina, G. Fernández-Varo, E. Casals, V. Reichenbach, G. Casals, B.G. de la Presa, S. Sandalinas, S. Carvajal, V. Puntes, W. Jiménez, Cerium oxide nanoparticles reduce steatosis, portal hypertension and display anti-inflammatory properties in rats with liver fibrosis, J. Hepatol. 64 (2016) 691–698.
[68] K. Levada, A. Omelyanchik, V. Rodionova, R. Weiskirchen, M. Bartneck, Magnetic-Assisted treatment of liver fibrosis, Cells 8 (2019) 1279.